Remote Sensing of Environment 125 (2012) 227–237

Contents lists available at SciVerse ScienceDirect

Remote Sensing of Environment

journal homepage: www.elsevier.com/locate/rse

Detecting rock glacier flow structures using Gabor filters and IKONOS imagery

Alexander Brenning [a,*], Shilei Long [a], Paul Fieguth [b]

[a] University of Waterloo, Department of Geography and Environmental Management, 200 University Avenue West, Waterloo, Ontario, Canada N2L 3G1
[b] University of Waterloo, Department of Systems Design Engineering, 200 University Avenue West, Waterloo, Ontario, Canada N2L 3G1

ARTICLE INFO

Article history:
Received 16 August 2011
Received in revised form 29 June 2012
Accepted 11 July 2012

Keywords:
Texture filters
Gabor filter
Terrain analysis
Multispectral remote sensing
Rock glacier
Debris-covered glacier
Flow patterns

ABSTRACT

While ridges and furrows on the surface of rock glaciers are probably the most characteristic morphological features of this expression of creeping mountain permafrost, this is the first study that examines the utility of texture filters in detecting rock glacier flow structures. Texture features were derived from a Gabor filterbank applied to two panchromatic IKONOS orthoimages from the Chilean Andes, and terrain attributes were obtained in order to narrow down the area of interest and as additional predictor variables. Four classification methods of different complexity (generalized linear model, GLM; generalized additive model, GAM; support vector machine, SVM; Bundling) were applied to three sets of predictor variables (texture attributes, terrain attributes, and the combination of both), and predictive performances were estimated using two spatial cross-validation strategies in terms of the median area under the ROC (receiver operating characteristics) curve (AUROC). Overall, classifiers utilizing texture attributes alone or, usually even better, in combination with terrain attributes outperformed terrain attributes alone, and Bundling (in most cases followed by SVM) showed the overall best performance as a classification method. Cross-validated median AUROC values were mostly between 0.70 and 0.80, or "fair," in this focused pilot study, but much better results are to be expected at the landscape scale. Permutation-based spatial variable importance measures indicate that Gabor features corresponding to texture wavelengths between 10 and 30 m are the most important predictors, which is consistent with typical ridge spacing on rock glaciers. Confounding occurred mostly in areas with linear erosion features and ridges or scarps in morainic and thermokarst terrain. We suggest that texture filters and the chosen methodological approach are relevant not only for rock glacier mapping but also for delineating debris-covered glaciers and characterizing glacier surfaces, as well as for other geomorphological and cryospheric applications.

1. Introduction

Rock glaciers are cryospheric features that are difficult to detect in remote-sensing imagery because their ice content is generally not exposed at the surface, limiting the utility of optical remote-sensing data for their automatic detection. Similar problems are encountered with debris-covered glaciers. Recent research has focused mostly on the combination of terrain attributes derived from digital elevation models with multispectral optical and/or thermal satellite remote sensing in order to detect ice-debris systems, in particular rock glaciers (Brenning, 2009; Janke, 2001; Piatek, 2009) and debris-covered glaciers (Bishop et al., 2001; Bolch et al., 2008; Kargel et al., 2005; Paul et al., 2004; Shukla et al., 2010). Although each of these approaches offers some level of discrimination between ice-debris systems and their surroundings, classification accuracies still need to be improved, especially in the case of rock glaciers, which are important ice storage systems especially in dry high-mountain areas (Azócar & Brenning, 2010).

Texture filters as an alternative approach to this problem have not yet been studied in this context, and are the focus of this paper. Active rock glaciers, as the geomorphic expression of ice-rich creeping mountain permafrost, typically present characteristic surface patterns with arcuate furrows and ridges as a result of several external and internal factors including their deformation (Barsch, 1996; Haeberli et al., 2006; Kääb & Weber, 2004). Ridges are typically 1–5 m high and between 10 and 100 m apart from each other, often with substantial variation within a rock glacier as well as within a mountain region (Kääb & Weber, 2004).

Gabor filters, as one particular class of texture filters, are a state-of-the-art approach to detecting and discriminating textures, particularly zebra-like or periodic band patterns, from a grayscale image or spectral band (Arivazhagan et al., 2006; Bovik et al., 1990). The Gabor function is a local matched filter, a tunable function parameterized by orientation, frequency, and wavelength. In the remote-sensing context, Gabor filters have been used to differentiate urban land uses (Xiao et al., 2010), and our expectation is that they are

* Corresponding author. Tel.: +1 519 8884567x35783; fax: +1 519 7460658.
E-mail address: brenning@uwaterloo.ca (A. Brenning).

0034-4257/$ – see front matter © 2012 Elsevier Inc. All rights reserved.
doi:10.1016/j.rse.2012.07.005

also useful for detecting flow structures in cryospheric features as well as in lava streams, for example.

Our objective is to assess the utility of Gabor filters in the detection of flow patterns of rock glaciers. We therefore apply state-of-the-art statistical and machine-learning classifiers to features obtained from a Gabor filterbank and determine their performance using cross-validation. The filter parameters that contribute the most to the predictive performance are furthermore determined using a permutation-based variable accuracy importance measure. We apply Gabor filters to the panchromatic band of IKONOS imagery (1 m×1 m resolution) of two study areas in the Chilean Andes.

2. Materials and methods

After introducing the study areas (Section 2.1) and image acquisition (Section 2.2) at the beginning of this section, we present the texture filters (Section 2.4) and terrain analysis processing steps, including the definition of a more focused area of interest (AOI) within the study areas based on a thresholding of terrain attributes (Section 2.3).

Terrain attributes are used to narrow the study region to a relevant area of interest (AOI); within the AOI terrain attributes are further used as additional predictor variables and as a set of benchmark predictors to which the Gabor-based performance can be compared.

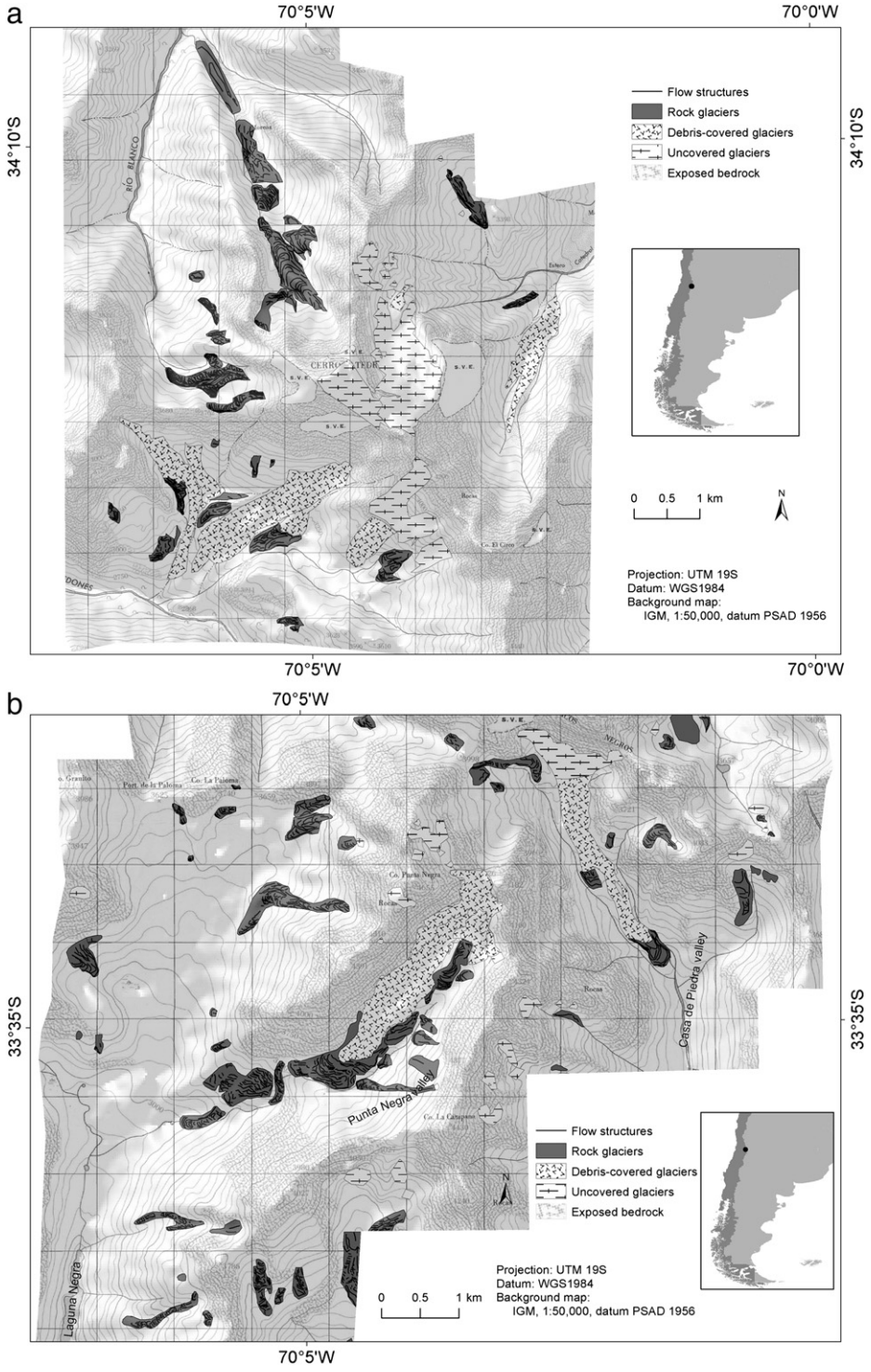

Fig. 1. Rock glaciers and glaciers in the Catedral (CAT; a) and Laguna Negra area (LAG; b) areas.

2.1. Study areas and 'ground truth'

Two study areas in the Western Main Cordillera of the Andes of Santiago are considered in this study. The distribution and characteristics of cryospheric features in both areas, which will be referred to as the Catedral (CAT) and Laguna Negra (LAG) areas, were studied previously in the field and from aerial photographs (Fig. 1; Brenning, 2005; Bodin et al., 2010). Active rock glaciers in these areas are abundant above 3500 m a.s.l., and active as well as inactive ones reach down to 3000–3200 m a.s.l. Some of the more prominent rock glaciers in the study areas are associated with debris-covered glaciers above 3200–3600 m a.s.l., which transition into uncovered glaciers at ~3800 m a.s.l. (Bodin et al., 2010; Brenning, 2005). Late Cretassic to Tertiary, mainly dark volcanic rocks are the most common rock types especially in the LAG area, where some exposures of Tertiary granodioritic intrusives are also present; in the CAT area, Late Cretassic sedimentary rocks are also present, including limestone deposits (Farías et al., 2008; Fock et al., 2005).

Rock glaciers were digitized from the available IKONOS orthoimagery (see Section 2.2.). Both areas had previously been mapped in the field. The CAT study area presents more than 25 rock glaciers, while the LAG area has more than 50 rock glaciers, the exact numbers depending on how multi-part landforms are counted.

Since rock glacier surface structures are not always well developed and the rooting zone of rock glaciers often presents a gradual transition into a talus slope, we decided to focus this pilot study on the detection of areas having a presence of flow structures within a rock glacier rather than the entire rock glacier polygons. By 'flow structures' we refer collectively to a wide range of linear to elliptical ridges and furrows on rock glaciers that may be related not only to different processes such as bulging and overthrusting, but also to freeze/thaw activity (Burger et al., 1999; Kääb & Weber, 2004). Flow structures on rock glaciers were digitized as polylines based on the visual interpretation of the IKONOS orthoimages (compare Fig. 2a). We refer to all areas within a rock glacier that are located within no more than 50 m from a digitized flow structure as 'areas with flow patterns.'

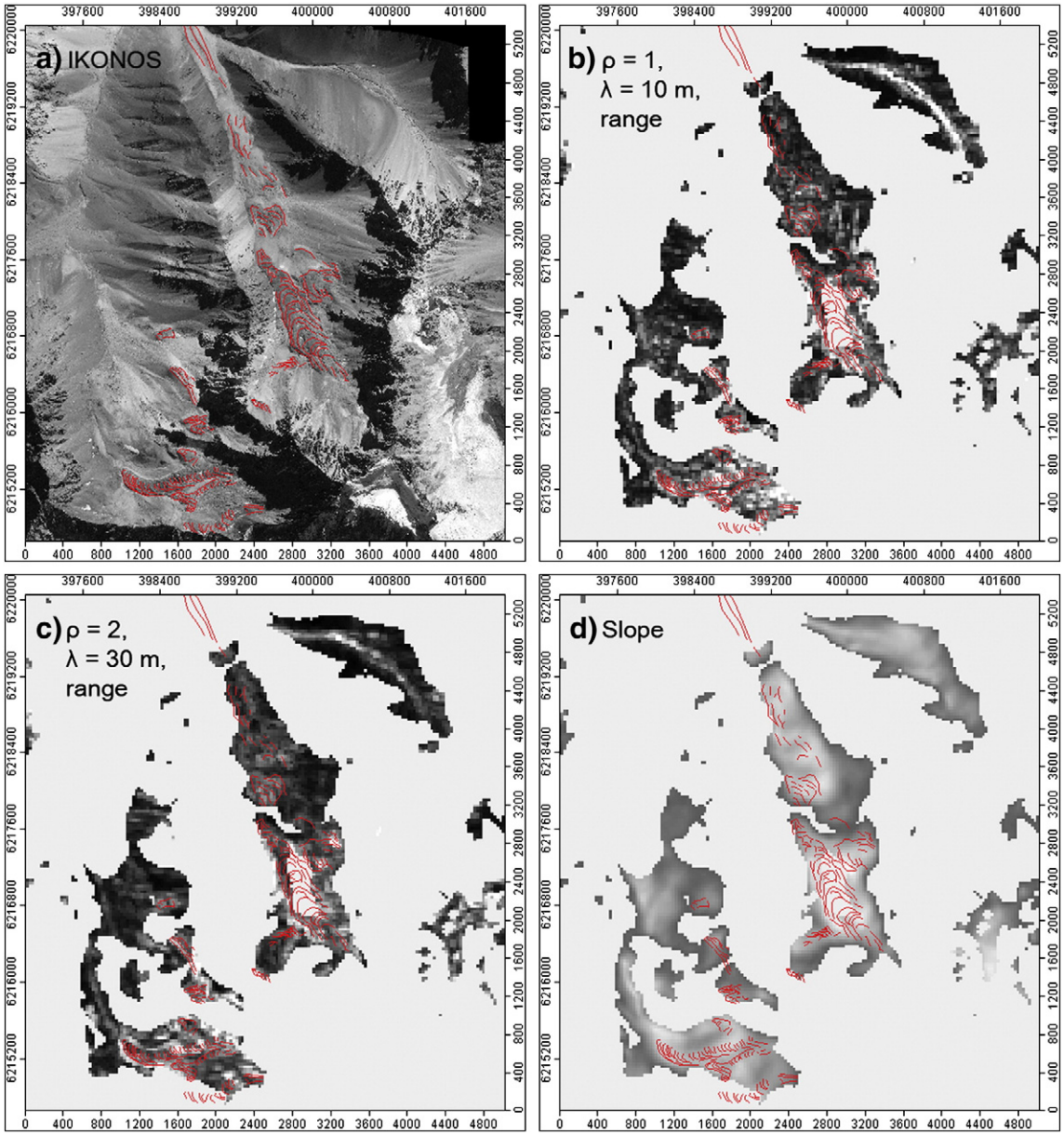

Fig. 2. Comparison of (a) IKONOS panchromatic imagery of part of the CAT area (shown with digitized flow structures), (b–c) selected Gabor features with high AUROC and SVI (b: $\rho = 1$, $\lambda = 10$ m, range; c: $\rho = 2$, $\lambda = 30$ m, range), and (d) slope angle. Linear gray scales have been adjusted for visual comparison; high values are bright, with the exception of slope. Masked areas correspond to unsuitable topography, bedrock, and uncovered glaciers/snow.

Rock glaciers occupy 13% of the CAT AOI and 15% of the LAG AOI defined below in Section 2.3. Of the rock glacier area of CAT, 83% exhibit flow patterns in the above sense, compared to 94% in LAG.

2.2. Remote-sensing imagery

Cloudless IKONOS imagery at the minimum snow extent was available for this study (CAT: April 5, 2008, 70 km^2; LAG: April 2, 2008, 67 km^2; GeoEye). IKONOS provides a panchromatic band at a 1 m×1 m resolution. Orthoimages (nominal horizontal root mean squared error of 5 m) were generated by Pacific Geomatics Ltd., Surrey, B.C. using a DEM of the Shuttle Radar Topography Mission (SRTM, version 3 from the Consultative Group for International Agriculture Research Consortium for Spatial Information, CGIAR, with filled gaps, vertical standard error 15–16 m according to Kääb, 2005; resolution 3″, projected and resampled to a 90 m×90 m UTM grid) for CAT, and a merged airborne stereophotogrammetric and SRTM product for LAG (Bodin et al., 2010; resolution 5 m×5 m). Differential and handheld GPS points available for LAG match the orthoimage very well; positional errors and geometric distortions in the most rugged parts of the study area may exceed the reported error levels but do not affect our results as they were excluded from the AOI (Section 2.3.).

2.3. Terrain analysis and area of interest

Terrain attributes as proxies for geomorphic and hydrological processes that allow (or hamper) the development of rock glaciers at a specific location have been used to characterize the topographic and climatic niche of rock glaciers and to predict their potential distribution on a regional scale (e.g., Brenning et al., 2007; Janke, 2005; Johnson et al., 2007; Brenning, 2009; Brenning & Azócar, 2010). Based on these studies, six terrain attributes including elevation itself (*ELEV* in m a.s.l., as a proxy of past and present-day mean annual air temperature, MAAT) were selected as predictor variables and derived from the ASTER GDEM product (source: Earth Remote Sensing Data Analysis Center; resolution 1″, projected and resampled to a 30 m×30 m UTM grid) using the SAGA GIS software (version 2.0.4; Conrad, 2006) and the 'RSAGA' and 'RPyGeo' packages in R (Brenning, 2008). Local slope (*SLP*, in degrees) was calculated using the algorithm of Zevenbergen and Thorne (1987). The logarithmic size of the upslope contributing area (*LCAREA*, $\log_{10}$ m^2) and the catchment slope (*CSLP*, degrees) and its logarithmic height (*LCHGT*, $\log_{10}$ m) were obtained with the multiple flow direction algorithm (Quinn et al., 1991). All-year potential incoming solar radiation (*PISR*, kWh m^{-2}) was calculated in SAGA GIS using a lumped atmospheric transmittance model (70% transmittance, daily calculation with 30-minute time steps).

In order to narrow down the AOI, topographic positions that are clearly unsuitable for the presence of rock glaciers were excluded. Following Brenning and Azócar (2010), eligible grid cells were required to fall within local altitudinal limits (here, 3000–4000 m a.s.l.), and have $SLP<30°$, $15°<CSLP<40°$ and 10^4 m$^2<LCAREA<10^{6.5}$ m^2. In addition, exposed bedrock areas were removed based on information digitized from topographic maps (scale 1:50,000, Instituto Geográfico Militar), and uncovered glaciers and snowbanks were masked out using a glacier mask derived by thresholding of IKONOS brightness values (bands 2 and 4). Digitized debris-covered glacier areas were furthermore removed in order to focus this study on differences between rock glacier flow structures and debris surfaces that are not moving. The remaining area is referred to as AOI throughout this paper.

Thus, only about one-fifth of the image area (CAT AOI: 12 km^2; LAG AOI: 15 km^2; Fig. 2) was actually used in this targeted analysis. The predictive accuracies obtained with this study design will naturally be significantly lower than results that would be obtained at the landscape scale.

2.4. Texture analysis

Gabor filters are motivated by the notion of textures as irradiance patterns with dominant spatial frequencies that characterize and differentiate distinct textures (Bovik et al., 1990; Clausi & Jernigan, 2000). The Gabor filter output is computed as the two-dimensional convolution of an image with a Gabor function, a local, tapered sinusoid. The two-dimensional Gabor functions have tunable orientations, frequencies, and extent, which can be used to detect and/or differentiate a certain range of pattern types or a narrowly defined distinct periodic feature. In this study, we combine Gabor functions covering all orientations, and apply them to the panchromatic channel of IKONOS imagery.

The Gabor filter function is the product of a Gaussian function and a complex sinusoid,

$$G(x,y,\theta,\varphi) = \exp\left(-\left(x'^2+y'^2\right)/\left(2\sigma^2\right)\right)\left(\cos(2\pi\varphi x') + i\sin(2\pi\varphi y')\right) \quad (1)$$

where (x,y) is the spatial location (in meters relative to the kernel's origin), φ is the spatial frequency (in cycles per meter, m^{-1}), σ is the standard deviation of the Gaussian weight function, and $i=(-1)^{1/2}$ is the imaginary number (compare Bovik et al., 1990). The pattern orientation θ appears implicitly, in that (x', y') represents that spatial location of (x,y) rotated by θ. In practice, the function G is truncated to a finite-sized window as explained below. Gabor filters were implemented in MATLAB® (The MathWorks, Inc., version 7.10) based on a two-dimensional discrete convolution. Only the real part of the convolution was used in this study.

Since no prior assumptions on the orientation of flow patterns in geographical space or with respect to topographic patterns can be made, Gabor filters were calculated for eight different directions (i.e., 22.5° steps of θ), and the minimum, maximum, range (maximum minus minimum) and median values were calculated over these eight directions. The motivation for including the range was that near-linear patterns can be expected to produce a larger range than near-circular patterns such as those generated by remnant snow patches or melt-out depressions.

Based on the typical spacing of ridges and furrows on the surface of rock glaciers in general and in the study area in particular, Gabor filters were calculated for pattern wavelengths of $\lambda=\varphi^{-1}=5$, 10, 20, 30, and 50 m on finite-sized moving windows of size 4.5λ×4.5λ. The choice of 2.25 complete cycles in each direction is specifically for the cosine in Eq. (1) to cross zero at the kernel boundary, greatly reducing boundary effects and edge artifacts for 0°- or 90°-oriented filters. A standard deviation of $\sigma=0.83$ was chosen, which results in an amplitude reduction to 0.48 at a distance of λ from the origin, 0.05 at 2λ, achieving a negligible amplitude at the filter borders (<0.03).

Flow patterns on rock glaciers are often rather heterogeneous, as ridge heights and spacing may change in response to compressive flow and overthrusting (Kääb & Weber, 2004), while each ridge tends to be relatively regular over longer distances. Elliptical Gabor filters were therefore used as a modification of Eq. (1) in which y' in the exponential function is replaced with $\rho y'$, where two possible values $\rho=1$, 2 were chosen as the axis ratio.

Filter values were aggregated in a final step to a 30 m×30 m grid resolution in order to match the geographical scale of the study as well as the DEM resolution. A maximum filter appeared to be the natural choice and was used for this purpose, since the flow structures would be thought of as being present within a 30 m×30 m grid cell if they were present at any point within the cell.

Thus, from a total of 320 individual Gabor filters we derived 40 Gabor filter features corresponding to five different wavelengths ($\lambda=5$, 10, 20, 30, and 50 m), two different axis ratios ($\rho=1$, 2) and

four different aggregation schemes (minimum, maximum, range and median). These were used as predictor variables in this study.

2.5. Classifier comparison

The statistical analysis was aimed at identifying important predictor variables, and determining the predictive performance achieved by texture attributes alone and in combination with terrain attributes. The presence/absence of flow patterns was the primary response variable of interest.

Four statistical and machine-learning techniques were applied to assess the predictive capabilities of the mentioned terrain attributes and texture attributes. Only a subset of four of the methods compared by Brenning (2009) was used, focusing on methods that are widely used in geomorphological mapping, or that represent different major classes of models such as tree-based ensemble techniques and linear statistical approaches. Specifically, we applied (1) the generalized linear model (i.e. logistic regression) with stepwise forward variable selection (GLM), (2) the generalized additive model with stepwise forward variable selection (GAM; Hastie & Tibshirani, 1990), (3) the support vector machine with internal cross-validation for hyperparameter tuning (SVM; Moguerza & Muñoz, 2006), and (4) Bundling, i.e., the combination of bootstrap-aggregated classification trees (bagging) with an ancillary classifier (Hothorn & Lausen, 2005), here with penalized linear discriminant analysis (PLDA; Hastie et al., 1995) with default shrinkage penalty coefficient equal to 1. Model set-up and tuning were as in Brenning (2009), except that in the present work, Bundling used PLDA instead of stabilized linear discriminant analysis (SLDA) because it was more successful in the direct comparison with SLDA in the study of Brenning (2009). The reader is referred to Brenning (2009) and the cited literature for further details on the methods used.

Each classifier was trained and tested using texture attributes, terrain attributes, and the combination of both in order to assess the utility of each of these three sets of predictors for detecting flow patterns. Of particular interest was the performance improvement achieved by adding texture attributes to the set of terrain attributes.

Predictive performance assessment is based on the estimation of the area under the receiver operating characteristic (ROC) curve (*AUROC*). The *AUROC* is a value between 0.5 and 1 that measures the discrimination achieved by a diagnostic measure independently of a specific decision threshold (Zweig & Campbell, 1993). We do not report false-positive rate (FPR) at a fixed true-positive rate (TPR) as proposed by Brenning (2009) because it is not possible to generalize such estimates from our very focused AOI to a larger area; instead, we focus on the general predictive performance by using the AUROC.

These performance measures were estimated for each classifier and group of predictor variables using cross-validation. In *k*-fold cross-validation, the data set is first divided into *k* partitions, and the classifier is then trained on the combined data from all but one of these partitions while the remaining partition is held out for prediction and error estimation. Training and prediction are repeated for all *k* combinations of test and training partitions, and the performance measures are averaged over all partitions.

Since ordinary cross-validation is based on random partitioning, samples from the same rock glacier or talus slope may be placed in the same cross-validation partition, and the resulting performance measures would not reflect the predictive performance in a real-world situation, in which a classifier is applied to a nearby, but spatially disjoint study area. To emulate this more realistic situation, we estimated the AUROC using two spatial cross-validation approaches. The first one used the CAT and LAG areas as spatially disjoint partitions in a two-fold ($k=2$) cross-validation. This allows us to assess the transferability of a classifier between relatively remote (60 km apart) study areas in the same mountain range. We refer to this as *test-area cross-validation*. In the second approach, we assessed classifier performances separately within each of the sub-areas, CAT and LAG. For this purpose, the classification techniques were examined in each area separately using a five-fold cross-validation with spatial partitions. Partitions are generated with the *k*-means clustering algorithm (Ruß & Brenning, 2010a). We refer to this as *spatial cross-validation*.

Partitioning and estimation were repeated 100 times for different sets of randomly selected flow and non-flow points and different random seeds in the case of the *k*-means algorithm. We report the median of the cross-validation estimates over all repetitions, denoting them as $mAUROC_{spCV}$ for spatial cross-validation and $mAUROC_{tCV}$ in the case of test-area cross-validation.

Flow-structure absence samples were required to lie outside the rock glacier polygons, having a minimum distance of 50 m from digitized flow features in order to avoid edge effects in areas immediately adjacent to rock glaciers. Within each training partition, 500 flow and 500 non-flow grid cells were drawn randomly as a training sample, and a sample with the same proportions and up to this size was drawn from the smaller test partition.

AUROC performances of different classification models and feature sets were first compared using non-parametric Kruskal–Wallis tests, which test for the presence of differences among a set of variables. Wilcoxon–Mann–Whitney rank sum tests were then used within each area and feature set (or classifier) in order to test whether differences between feature sets (or classifiers, respectively) relative to the best-performing feature set (classifier) were significant. The Simes procedure was applied within each group of tests to account for multiple testing (Benjamini & Hochberg, 1995), ensuring that the false discovery rate (FDR) is controlled at $<5\%$.

All statistical analyses were conducted in the data analysis software R (version 2.11.1; R Development Core Team, 2010) with its contributed packages 'e1071' (Dimitriadou et al., 2007), 'gam' (Hastie, 2009), 'ipred' (Peters & Hothorn, 2009), 'mda' (Hastie & Tibshirani, 2009) and 'ROCR' (Sing et al., 2009).

2.6. Variable importance

It is generally difficult to assess the "importance" of a particular variable in a complex prediction model using multiple predictor variables. While approaches based on, for example, standardized regression coefficients, are available for particular model types, we choose a more recent technique that can be applied across all different model types selected for this study. This technique consists of determining how much a performance measure deteriorates if a particular variable is randomly permuted, or 'messed up' (Strobl et al., 2007). This intuitive and effective, but computationally demanding method is known as permutation-based variable accuracy importance. Ruß and Brenning (2010b) proposed the use of this method in a spatial cross-validation context in order to assess the contribution of a variable to the spatial predictive performance.

In this study, a permutation-based spatial variable importance (SVI) measure was obtained based on the AUROC and estimated within the test-area cross-validation. For each particular test partition, one variable at a time was permuted ten times, and for each permutation the AUROC of the resulting prediction was obtained. In each cross-validation repetition, the discrepancy in AUROC between permuted and undisturbed predictions was calculated, using a total of $2\times100\times10=2000$ permutations per variable. The result is standardized by dividing it by the value obtained for the strongest predictor variable; we denote this as the SVI_{tCV}. The SVI therefore expresses in relative terms the contribution of each variable to the improvement of discrimination in a spatially disjoint test area. The limitations of variable importance measures in the presence of correlations between multiple predictor variables need to be taken into account when interpreting them.

3. Results

3.1. Exploratory analysis

Terrain attributes and texture attributes were only weakly correlated, with absolute values of Spearman correlation coefficients of less than 0.40, indicating that both data sources provided complementary information. Strong correlation ($\rho \geq 0.80$) was present in 27 out of 780 pairs of texture attributes, essentially among pairs of variables corresponding to adjacent discrete values of the wavelength parameter λ (e.g., $\lambda = 20$ m versus $\lambda = 30$ m) or similar aggregation schemes (especially range and maximum aggregation of directional Gabor filters) with otherwise identical filter parameters.

Circular ($\rho = 1$) Gabor texture attributes corresponding to wavelengths between 10 m and 30 m showed the most promise in discriminating flow structures, based on univariate AUROC values mostly between 0.65 and 0.72 (Table 1; Figs. 2b–c; 3). For $\rho = 1$, maximum-based aggregation resulted in filter variables nearly identical to the corresponding range-based variable, and discrimination was marginally better according to univariate AUROC. With few exceptions (especially filters with $\rho = 2$ and median-based aggregation), the Gabor filters were at least weakly associated with the presence of flow patterns.

In a principal component (PC) analysis, the first three PCs concentrated 81% of the total variance of all texture attributes, while 12 PCs were required to represent 95% of their variance. Most of these 12 PCs showed almost no discrimination (AUROC < 0.55), while the first two PCs achieved AUROCs of 0.67 and 0.66. This suggests that an a priori data reduction as in principal-component logistic regression would likely discard important texture information, and other strategies for dealing with large numbers of partly highly correlated predictors are therefore needed and applied in this work.

Terrain attributes show different levels of association with the presence of flow structures (Table 2), slope angle (*SLP*) achieving the highest univariate AUROC of 0.79 (Figs. 2d; 3). In the case of *ELEV*, a non-monotonic relationship is present, which is not detected by the univariate AUROC analysis, but should be detectable for nonlinear models such as the GAM.

3.2. Classifier performance comparison

AUROC performances of classifiers using the combined texture and terrain attribute feature set were consistently higher than or at least as high as classifiers using only texture attributes, finally followed by classifiers using only terrain attributes, according to both test-area and spatial cross-validation (Tables 3, 4; Fig. 4a). When looking at individual classifiers, results of spatial cross-validation were more heterogeneous than results of test-set cross-validation. In spatial cross-validation, the combination of texture and terrain attributes performed better than terrain attributes in 7 out of 8 comparisons, but better than or equal to texture attributes in only 5 out of 8 comparisons (Table 4). Most pairwise comparisons of AUROCs achieved with different feature sets with the best-performing classifier within each area and classifier were significantly different at a FDR ≤ 5%, with the exception of four comparisons involving irrelevant median performance differences ≤ 0.003.

In the comparison of classifiers using each classifier's best-performing feature set, Bundling achieved the best median AUROC performance in test-area cross-validation and also in spatial cross-validation in the LAG area, but not in the CAT area where it ranked second after the GAM (Fig. 4b). SVM ranked second in test-area cross-validation as well as in spatial cross-validation in the LAG area. All classifiers achieved their best median AUROC performances with either the texture feature set or the combined feature set, with the exception of GLM in spatial cross-validation in the CAT area (Fig. 4b). Highest median AUROC values were between 0.724 and 0.818 in the different cross-validation scenarios (Fig. 4b). All pairwise comparisons of classifiers with the best-performing classifier within each area and feature set were significantly different at a FDR ≤ 5%, with only one exception (Bundling versus SVM in CAT for the combination of texture and terrain attributes).

Inconsistent and partly poor predictive performances of classifiers using only terrain attributes ($mAUROC_{spCV}$ between 0.540 and 0.770) can likely be attributed to the narrow topographic definition of the AOIs, which does not allow the classifiers to identify general, possibly nonlinear relationships as in studies using samples from the entire landscape (e.g., Brenning et al., 2007). This may also have contributed to the relatively inconsistent $mAUROC_{spCV}$ on the combined predictor set.

Bundling performed consistently better than the GAM in direct comparisons using the same feature set, and the GAM was also slightly better than GLM in terms of median AUROC values obtained in all three scenarios (Tables 3, 4).

The SVM did not fit into this simple pattern. It performed quite well in many situations but poorly with two feature sets in test-area cross-validation and with one in spatial cross-validation (Tables 3, 4). This can possibly be attributed to uncertainties and algorithm instability in internal hyperparameter tuning with limited training data. This is especially true for test-area cross-validation, where no similar "remote" test area was available for internal hyperparameter tuning, but instead the training area (CAT or LAG) had to be partitioned spatially for this internal cross-validation step. In fact a look at the optimal hyperparameters in test-area cross-validation replications of the SVM shows that models trained in one area had optimal hyperparameters $C = 100$ and $\gamma = 0.0032$ (training-set AUROC approx. 0.78), while training in the other area yielded an optimal $C = 0.032$ and $\gamma = 0.0001$ (training-set AUROC ≈ 0.85), resulting in a very different predictive behavior. In contrast to this, optimal hyperparameters differed very little between different training areas when the SVM was applied to terrain attributes alone or in combination with texture attributes in test-area cross-validation.

In qualitative terms, the comparison of digitized flow patterns and modeled probabilities of their occurrence shows mixed results, with some flow patterns being depicted quite well and others not (Fig. 5). Debris-covered glaciers, which were removed from the AOI considered here, were often also highlighted by the predicted probabilities. Although their dynamics are usually different, multiple generations of lateral moraine ridges may produce similar patterns as the ones observed on rock glaciers. Melt-out depressions that are separated by remnant debris ridges and hummocks may exhibit linear to elliptical scarps that are not distinguishable from rock glacier flow structures with the filters used. Debris-flow channels and similar linear features on talus slopes and alluvial cones are also sometimes highlighted by the Gabor features used, in particular in the raw filter images prior to the spatial aggregation step.

Table 1
Capability of texture attributes to discriminate flow patterns expressed as univariate AUROC values on the merged CAT/LAG data set.

Filter parameters	Type of angular aggregation			
	Minimum	Maximum	Range	Median
$\rho = 1, \lambda = 5$ m	0.652	0.663	0.665	0.656
$\rho = 1, \lambda = 10$ m	0.682	0.691	0.690	0.691
$\rho = 1, \lambda = 20$ m	**0.706**	0.697	0.696	**0.717**
$\rho = 1, \lambda = 30$ m	**0.708**	0.692	0.692	**0.712**
$\rho = 1, \lambda = 50$ m	0.676	0.655	0.655	0.676
$\rho = 2, \lambda = 5$ m	0.501	0.634	0.672	0.553
$\rho = 2, \lambda = 10$ m	0.513	0.654	0.691	0.555
$\rho = 2, \lambda = 20$ m	0.530	0.654	**0.707**	0.556
$\rho = 2, \lambda = 30$ m	0.549	0.631	**0.703**	0.532
$\rho = 2, \lambda = 50$ m	0.567	0.590	0.668	0.502

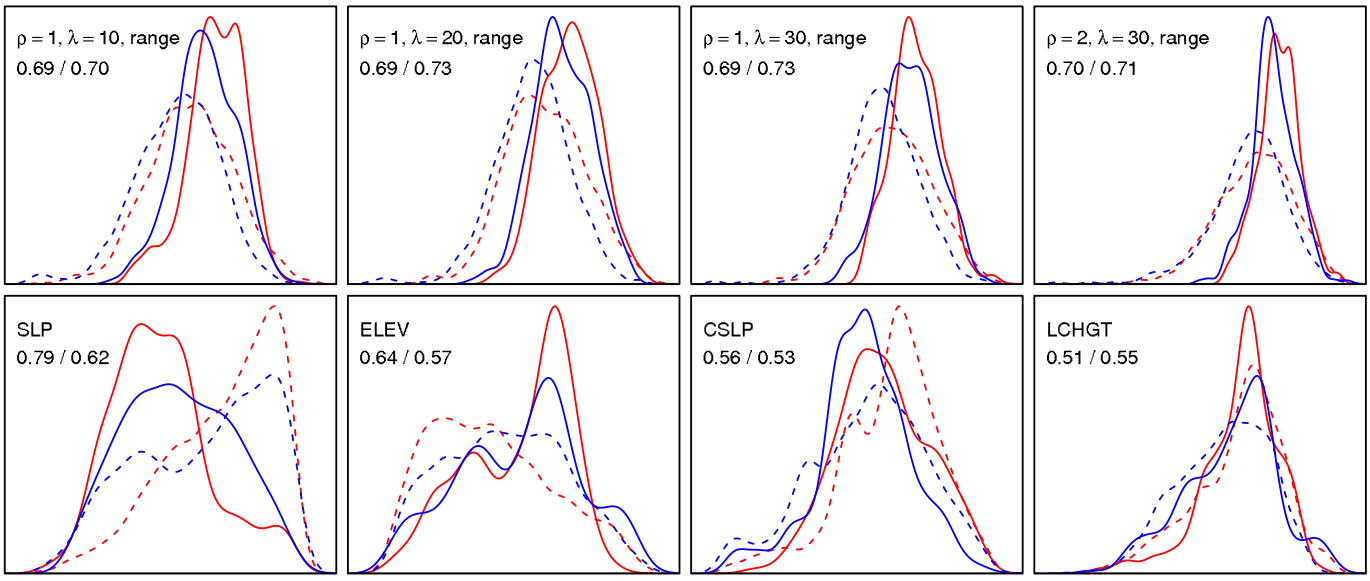

Fig. 3. Empirical probability densities of texture and terrain attributes with highest SVI for flow patterns (solid lines) and areas without flow patterns (dashed). Red lines represent the CAT area and blue lines LAG; numbers indicate AUROC in CAT/LAG. Kernel density estimates calculated with Gaussian kernel and bandwidth chosen according to Silverman's rule of thumb.

It should be noted that AUROC performances are deflated on our data sets because of the specific sampling and matching design, which was intended to eliminate areas that are clearly irrelevant for rock glacier development. Without these masking steps, Bundling, for example, would indeed achieve a $mAUROC_{tCV}$ of 0.885 (instead of 0.724) in our study using the combination of texture and terrain attributes.

3.3. Variable importance

The results of the variable importance assessment are shown in Table 5 for the combination of terrain and texture attributes. Apart from slope (*SLP*), which had the highest SVI in three of the four classification techniques, only elevation (*ELEV*) and catchment slope (*CSLP*) achieved an SVI above 0.15 in at least one method, specifically in Bundling.

The strongest texture attributes had wavelength parameters predominantly of 20 and 30 m, but also of 10 m (ranked second) and, at lower ranks, 5 m and 50 m. Filter variables with range aggregation were more dominant in the higher SVI ranks than other directional aggregation schemes, especially compared to minimum aggregation (rank 11, highest SVI 0.30). Most variables with SVI≥0.15 were strong only in one classification method, with the exception of the $\rho = 1$, $\lambda = 30$ m Gabor filter with median aggregation, and, to a lesser extent, the $\rho = 1$, $\lambda = 10$ m filter with range.

Interestingly, one of the Gabor filter variables that showed no discrimination in univariate AUROC analysis ($\rho = 2$, $\lambda = 5$ m, minimum aggregation; AUROC 0.50) was among the more important variables in the GLM and Bundling models. Also, *CSLP* was somewhat important in the more complex, interactive models SVM and Bundling, despite showing extremely weak discrimination in the univariate analysis. This underlines the notion that predictor variables should not be discarded a priori based on univariate scores or based on the small contribution of a principal component to the total variance of the predictors. Especially machine-learning methods that are specifically designed for detecting nonlinear or interactive relationships in high-dimensional data may still be able to extract useful decision criteria from such data. On the other hand, these observations highlight the fact that variable importance strongly depends on how well the data characteristics such as a variable's distribution and the type of the relationship with the response variable (e.g., linear, nonlinear or interactive) match the capabilities of a specific classification method.

SVI was distributed more equally over a larger number of variables in SVM and especially Bundling compared to GLM and GAM. Both GLM and GAM used stepwise variable selection procedures (and the GAM an additional variable preselection because of software limitations), which results in models effectively using only a small subset of the available variables. Since training sets in test-area cross-validation varied very little, very similar sets of variables were selected in each training area across all cross-validation repetitions. Bundling, by contrast, is based on averaging many trees built on different (non-spatially) random subsets of the data, which will likely make use of all variables at some point.

4. Discussion

The automatic detection of rock glaciers – and also of debris-covered glaciers – still constitutes a major challenge. Research has

Table 2
Descriptive summary statistics (median and interquartile range) of terrain attributes and their capability to discriminate flow patterns on the merged CAT/LAG data set.

Variable	Flow samples	Non-flow samples	AUROC
ELEV	3571 (325)	3379 (367)	0.624
SLP	14.0 (7.1)	22.9 (9.7)	0.792
CSLP	29.9 (5.8)	31.2 (6.3)	0.555
LCAREA	4.73 (0.68)	4.59 (0.55)	0.582
LCHGT	2.48 (0.21)	2.48 (0.31)	0.504
PISR	1998 (188)	1880 (291)	0.653

Table 3
Test-area cross-validation AUROC ($AUROC_{tCV}$) for four classification techniques using texture attributes, terrain attributes, and the combination of both: Median of AUROC measured over all cross-validation repetitions.

Model	Texture attributes	Terrain attributes	Texture and terrain attributes
GLM	0.673	**0.661**	0.674
GAM	0.697	0.618	0.697
SVM	0.575	0.530	0.716
Bundling	**0.713**	0.617	**0.724**

AUROC of best-performing classifier in each column printed in boldface.

Table 4
Spatial cross-validation AUROC ($mAUROC_{spCV}$) for four classification techniques using texture attributes, terrain attributes, and the combination of both: Median values over all cross-validation repetitions in the CAT/LAG areas.

Model	Texture attributes	Terrain attributes	Texture and terrain attributes
GLM	0.640/0.711	**0.770**/0.578	0.756/0.685
GAM	0.722/0.729	0.737/0.630	**0.818**/0.732
SVM	0.751/0.786	0.540/0.573	0.778/0.766
Bundling	**0.796**/**0.793**	0.572/**0.647**	0.771/**0.795**

AUROC of best-performing classifier in each column printed in boldface.

so far focused mainly on the combination of multispectral optical remote sensing from the visible spectrum to thermal wavebands with geomorphometric information. To our knowledge, this is the first study that utilizes texture filters in order to identify ice-debris landforms based on their surface texture. This may seem surprising given the fact that the ridges and furrows on the surface of rock glaciers are "the most characteristic feature of rock glacier morphology mentioned by observers, [which] can be used to identify rock glaciers in both the field and on aerial photographs" (Burger et al., 1999), and that debris-covered glaciers also typically present surface topography features related to ablation and deformation processes (Bodin et al., 2010; Clayton, 1964).

Overall, our results confirm that Gabor filters show promise for mapping rock glaciers, and suggest that they have some potential for mapping related surface features in mountain areas as well, especially debris-covered glaciers, subject to local calibration. Texture filters will be most effective if applied in combination with several other classification approaches and data sources. In the context of ice-debris landforms, multispectral sensors in the visible and near-infrared can be used to mask out vegetation, uncovered glaciers and snowfields, and water surfaces. Terrain attributes are especially useful to discard most, though not all, areas of exposed bedrock, as well as areas that are topographically unsuitable for the development of an ice-debris landform (Brenning & Azócar, 2010). Elevation as a proxy for MAAT plays a particular role as it allows us to focus on a particular climatic niche of cryospheric features. These DEM-based criteria alone may typically be used to mask out between one-third and two-thirds of a mountain area. Landscape-scale classification would therefore likely achieve AUROC values on the order of 0.85–0.95 (Brenning & Azócar, 2010).

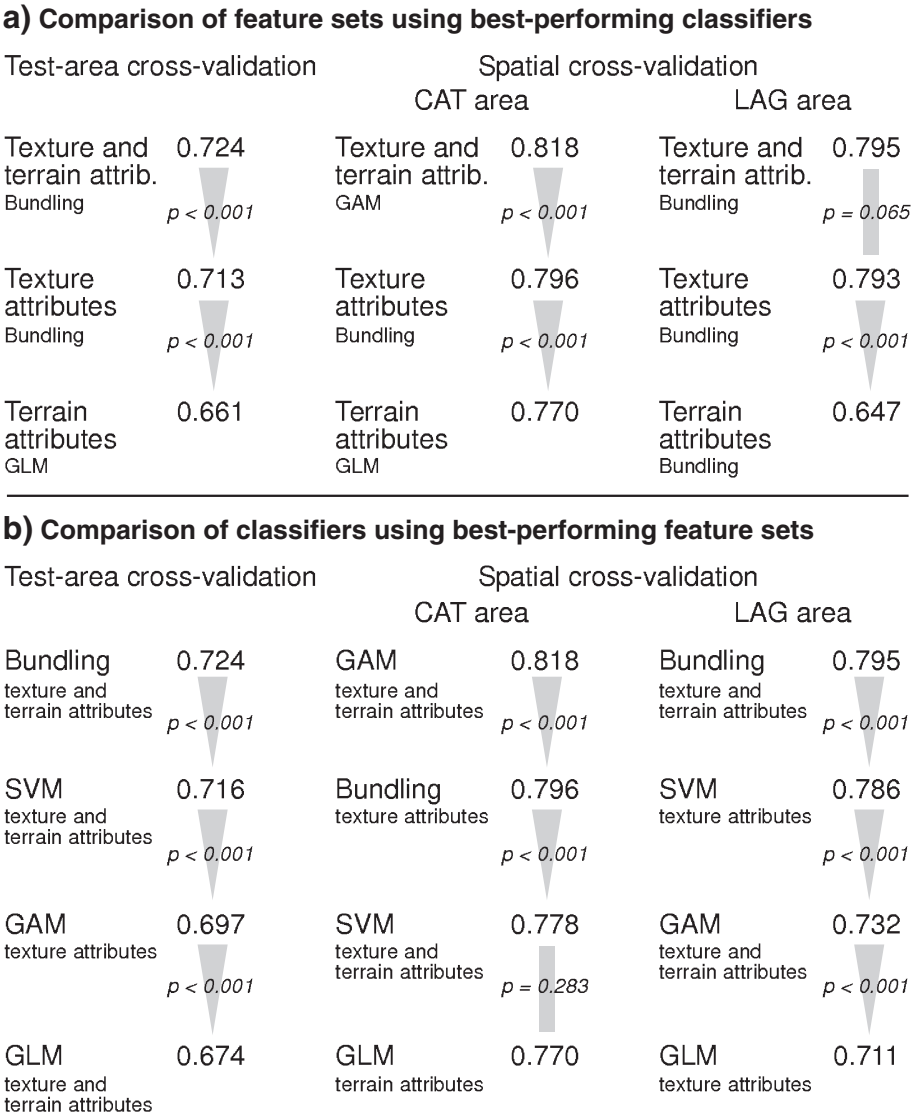

Fig. 4. Synthesis of differences in median AUROC predictive performances among different feature sets and different classifiers. (a) Comparison of mAUROC performances achieved by different feature sets using each feature set's best-performing classifier. (b) Comparison of mAUROC performances of different classifiers each using its best-performing feature set (compare Tables 3 and 4). Indicated unadjusted *p*-values correspond to Wilcoxon–Mann–Whitney tests.

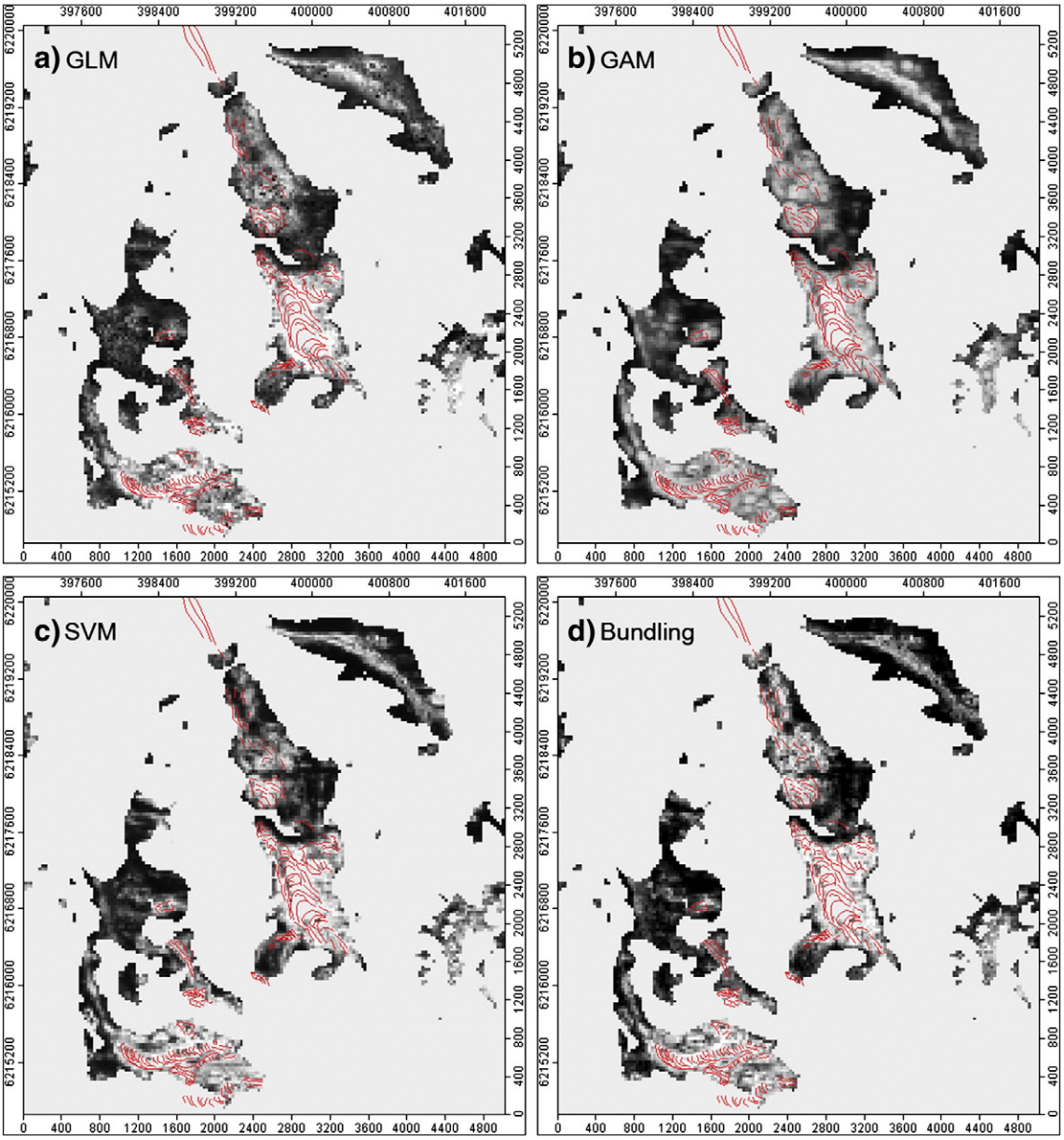

Fig. 5. Comparison of model predictions generated by the four models trained on combined terrain attribute and texture feature data. Models were trained on a training sample from the combined CAT and LAG areas. Linear gray scales have been adjusted for visual comparison; high values are bright. Masked areas correspond to unsuitable topography, bedrock, and uncovered glaciers/snow.

Several practical recommendations can be derived from our results. Future studies on the detection of rock glaciers with similar characteristics using Gabor filters may focus on filter wavelengths λ between 10 and 30 m. Even though larger flow structures were present in our study areas, their replication was more limited, and larger kernels will more likely cover multiple surface types, resulting in artifacts near the boundaries of a landform, which reduces their ability to discriminate different surface types. We recommend the use of the range aggregation of directional Gabor filters in future studies because it had the strongest SVI, or alternatively the simpler maximum aggregation, which resulted in features almost equivalent to those derived with range aggregation. An improved directional resolution (in this study, 22.5°) may further be beneficial. We finally conclude that preference can be given to isotropic Gabor features.

The need to select a classification method that is suitable to the specific image classification problem at hand has been emphasized before (Brenning, 2009; Marmion et al., 2008; Mountrakis et al., 2011) and was confirmed by our more limited comparison of four classifiers of different complexity. Here, the more complex Bundling and SVM classifiers outperformed the simpler GAM and GLM classifiers in most situations in which texture attributes were included in the set of predictors. The use of spatial cross-validation approaches ensured that the performance estimates are transferable to areas with similar characteristics (Brenning, 2005).

Texture filters and specifically Gabor filters show promise in numerous other applications of remote sensing (e.g., Recio-Recio et al., 2005; Xiao et al., 2010). In cryospheric research, they may be useful for detecting and differentiating surface structures on glaciers, which are related to specific dynamic characteristics of a glacier; geostatistical pattern-recognition approaches have been previously used for this purpose (Herzfeld et al., 2000). The recognition and characterization of patterned ground structures in high-latitude periglacial environments (Hjort & Luoto, 2006) is another potential application. However, Earth surface features with similar textures that exist in proximity to the feature of interest may result in potential confounding of landforms. In our context, some moraines and

Table 5
Spatial variable importance (SVI) based on changes in median AUROC using test-area cross-validation ($mAUROC_{tCV}$). Values are standardized relative to the most important predictor of each classifier. Only variables with SVI≥0.15 in at least one classifier are shown.

Variable name/ Gabor parameters	Rank	Highest SVI	GLM	GAM	SVM	Bundling
SLP	1	**1.00**	**0.47**	**1.00**	**1.00**	**1.00**
$\rho=1$, $\lambda=10$ m, range	2	**1.00**	**1.00**	0.16	0.11	0.34
$\rho=1$, $\lambda=20$ m, range	3	**0.91**	0.06	**0.91**	0.12	0.11
$\rho=1$, $\lambda=30$ m, range	4	0.83	0.05	**0.83**	0.09	0.18
$\rho=2$, $\lambda=30$ m, range	5	0.82	0.11	0.82	0.03	0.20
$\rho=1$, $\lambda=30$ m, median	6	0.52	0.27	0.20	**0.52**	**0.35**
$\rho=1$, $\lambda=5$ m, range	7	0.34	0.09	0.00	0.04	**0.34**
$\rho=2$, $\lambda=20$ m, range	8	0.34	**0.34**	0.13	0.19	0.14
$\rho=1$, $\lambda=20$ m, maximum	9	0.33	0.01	0.33	0.05	0.10
$\rho=1$, $\lambda=50$ m, range	10	0.32	0.09	0.32	0.06	0.28
$\rho=2$, $\lambda=5$ m, minimum	11	0.30	0.30	0.00	0.20	0.09
$\rho=1$, $\lambda=50$ m, median	12	0.27	0.06	0.05	**0.27**	0.18
$\rho=1$, $\lambda=20$ m, median	13	0.23	0.16	0.09	0.23	0.17
$\rho=2$, $\lambda=5$ m, range	14	0.23	0.23	0.00	0.04	0.14
ELEV	15	0.19	0.09	0.01	0.13	0.19
CSLP	16	0.18	0.08	0.00	0.12	0.18
$\rho=1$, $\lambda=30$ m, maximum	17	0.17	0.00	0.17	0.09	0.17
$\rho=1$, $\lambda=50$ m, maximum	18	0.16	0.04	0.16	0.11	0.07

The three highest SVI values of each classifier are printed in boldface.

debris-covered glaciers, but in some cases even lava streams may cause such problems (Fort, 2003). However, geomorphometric criteria may help discriminate different landform types with similar texture patterns.

5. Conclusions

Texture analysis methods and specifically Gabor filters are one step forward towards the automatic detection of rock glacier flow structures from remote-sensing imagery. Isotropic Gabor filters with wavelength parameters that are consistent with rock glacier ridge distances appear to be preferable. Gabor filters also show promise for mapping debris-covered glaciers and other landforms with characteristic surface patterns but little spectral discrimination. These filters are best applied in combination with terrain attributes as proxies for geomorphological and climatic processes controlling the presence of these landforms. In our study, the use of flexible machine-learning techniques improved the spatial predictive utility and transferability of the texture attributes compared to linear and additive statistical models.

Acknowledgments

This research was funded through a NSERC Discovery Grant awarded to A. Brenning. It benefited greatly from discussions with M. Peña (Universidad Mayor, Santiago, Chile), which were made possible by funding from the International Development Research Centre's LACREG program. Constructive comments from three anonymous reviewers are gratefully acknowledged.

References

Arivazhagan, S., Ganesan, L., & Priyal, S. P. (2006). Texture classification using Gabor wavelets based rotation invariant features. *Pattern Recognition Letters*, *27*, 1976–1982. http://dx.doi.org/10.1016/j.patrec.2006.05.008.

Azócar, G. F., & Brenning, A. (2010). Hydrological and geomorphological significance of rock glaciers in the dry Andes, Chile (27°–33°S). *Permafrost and Periglacial Processes*, *21*(1), 42–53. http://dx.doi.org/10.1002/ppp. 669.

Barsch, D. (1996). *Rockglaciers: Indicators for the present and former geoecology in high mountain environments*. Berlin: Springer.

Benjamini, Y., & Hochberg, Y. (1995). Controlling the false discovery rate — A practical and powerful approach to multiple testing. *Journal of the Royal Statistical Society B*, *57*(1), 289–300.

Bishop, M. P., Bonk, R., Kamp, U., & Shroder, J. F. (2001). Terrain analysis and data modeling for alpine glacier mapping. *Polar Geography*, *25*, 182–201. http://dx.doi.org/10.1080/10889370109377712.

Bodin, X., Rojas, F., & Brenning, A. (2010). Status and evolution of the cryosphere in the Andes of Santiago (Chile, 33.5°S.). *Geomorphology*, *118*, 453–464. http://dx.doi.org/10.1016/j.geomorph.2010.02.016.

Bolch, T., Buchroithner, M. F., Kunert, A., & Kamp, U. (2008). Automated delineation of debris-covered glaciers based on ASTER data. In M. A. Gomarasca (Ed.), *GeoInformation in Europe. Proc. 27th EARSeL-Symposium, 4.-7.6.07, Bozen, Italy*. (pp. 403–410) Netherlands: Millpress.

Bovik, A. C., Clark, M., & Geisler, W. S. (1990). Multichannel texture analysis using localized spatial filters. *IEEE Transactions on Pattern Analysis and Machine Intelligence*, *12*, 55–73.

Brenning, A. (2005). Geomorphological, hydrological and climatic significance of rock glaciers in the Andes of Central Chile (33–35°S). *Permafrost and Periglacial Processes*, *16*, 231–240. http://dx.doi.org/10.1002/ppp. 528.

Brenning, A. (2008). Statistical geocomputing combining R and SAGA: The example of landslide susceptibility analysis with generalized additive models. In J. Böhner, T. Blaschke, & L. Montanarella (Eds.), *SAGA — Seconds out. Hamburger Beiträge zur Physischen Geographie und Landschaftsökologie*, *Vol. 19*. (pp. 23–32).

Brenning, A. (2009). Benchmarking classifiers to optimally integrate terrain analysis and multispectral remote sensing in automatic rock glacier detection. *Remote Sensing of Environment*, *113*, 239–247. http://dx.doi.org/10.1016/j.rse.2008.09.005.

Brenning, A., & Azócar, G. F. (2010). Statistical analysis of topographic and climatic controls and multispectral signatures of rock glaciers in the dry Andes, Chile (27°–33°S). *Permafrost and Periglacial Processes*, *21*, 54–66. http://dx.doi.org/10.1002/ppp. 670.

Brenning, A., Grasser, M., & Friend, D. (2007). Statistical estimation and generalized additive modeling of rock glacier distribution in the San Juan Mountains, Colorado, USA. *Journal of Geophysical Research - Earth Surface*, *112*, F02S15. http://dx.doi.org/10.1029/2006JF000528.

Burger, K. C., Degenhardt, J. J., Jr., & Giardino, J. R. (1999). Engineering geomorphology of rock glaciers. *Geomorphology*, *31*, 93–132. http://dx.doi.org/10.1016/S0169-555X(99)00074-4.

Clausi, D. A., & Jernigan, M. E. (2000). Designing Gabor filters for optimal texture separability. *Pattern Recognition*, *33*, 1835–1849. http://dx.doi.org/10.1016/S0031-3203(99)00181-8.

Clayton, L. (1964). Karst topography on stagnant glaciers. *Journal of Glaciology*, *5*(37), 107–112.

Conrad, O. (2006). SAGA — Program structure and current state of implementation. In J. Böhner, K. R. McCloy, & J. Strobl (Eds.), *SAGA — Analysis and modelling applications. Göttinger Geographische Abhandlungen*, *Vol. 115*. (pp. 39–52).

Dimitriadou, E., Hornik, K., Leisch, F., Meyer, D., & Weingessel, A. (2007). *e1071: Misc functions of the department of statistics (e1071), TU Wien. R package version 1.5-17.*

Farías, M., Charrier, R., Carretier, S., Martinod, J., Fock, A., Campbell, A., Cáceres, J., & Comte, D. (2008). Late Miocene high and rapid surface uplift and its erosional response in the Andes of central Chile (33°–35°S). *Tectonics*, *27*, TC1005. http://dx.doi.org/10.1029/2006TC002046.

Fock, A., Charrier, R., Farías, R., Maksaev, V., Fanning, M., & Álvarez, P. (2005). Exhumation and uplift of the western Main Cordillera between 33° and 34°S. *Extended abstracts, 6th International Symposium on Andean Geodynamics, ISAG 2005, Barcelona, Spain* (pp. 273–276).

Fort, M. (2003). Are high altitude, lava stream-like, debris mixtures all rock glaciers? A perspective from the Western Himalaya. *Zeitschrift für Geomorphologie, Supplementband*, *130*, 11–29.

Haeberli, W., Hallet, B., Arenson, L., Elconin, R., Humlum, O., Kääb, A., Kaufmann, V., Ladanyi, B., Matsuoka, N., Springman, S., & Vonder Mühll, D. (2006). Permafrost creep and rock glacier dynamics. *Permafrost and Periglacial Processes*, *17*, 189–214. http://dx.doi.org/10.1002/ppp. 561.

Hastie, T. (2009). GAM: Generalized additive models. R package version 1.01. http://CRAN.R-project.org/package=gam

Hastie, T. J., Buja, A., & Tibshirani, R. (1995). Penalized discriminant analysis. *The Annals of Statistics*, *23*(1), 73–102.

Hastie, T. J., & Tibshirani, R. (1990). *Generalized additive models*. London: Chapman & Hall.

Hastie, T., & Tibshirani, R. (2009). MDA: Mixture and flexible discriminant analysis. R package version 0.4-1, R port by F. Leisch, K. Hornik & B. D. Ripley. http://CRAN.R-project.org/package=mda

Herzfeld, U. C., Mayer, H., Feller, W., & Mimler, M. (2000). Geostatistical analysis of glacier-roughness data. *Annals of Glaciology*, *30*(1), 235–242. http://dx.doi.org/10.3189/172756400781820769.

Hjort, J., & Luoto, M. (2006). Modelling patterned ground distribution in Finnish Lapland: An integration of topographical, ground and remote sensing information. *Geografiska Annaler*, *88A*, 19–29.

Hothorn, T., & Lausen, B. (2005). Bundling classifiers by bagging trees. *Computational Statistics & Data Analysis*, *49*(4), 1068–1078. http://dx.doi.org/10.1016/j.csda.2004.06.019.

Janke, J. R. (2001). Rock glacier mapping: A method utilizing enhanced TM data and GIS modeling techniques. *Geocarto International*, *16*(3), 5–15.

Janke, J. (2005). The occurrence of alpine permafrost in the Front Range of Colorado. *Geomorphology*, *67*, 375–389. http://dx.doi.org/10.1016/j.geomorph.2004.11.005.

Johnson, B. G., Thackray, G. D., & Van Kirk, R. (2007). The effect of topography, latitude, and lithology on rock glacier distribution in the Lemhi Range, central Idaho, USA. *Geomorphology*, *91*, 38–50. http://dx.doi.org/10.1016/j.geomorph.2007.01.023.

Kääb, A. (2005). *Remote sensing of mountain glaciers and permafrost creep. Schriftenreihe Physische Geographie*, *48*, Zürich: University of Zürich.

Kääb, A., & Weber, M. (2004). Development of transverse ridges on rock glaciers: Field measurements and laboratory experiments. *Permafrost and Periglacial Processes*, *15*, 379–391. http://dx.doi.org/10.1002/ppp. 506.

Kargel, J. S., Abrams, M. J., Bishop, M. P., Bush, A., Hamilton, G., Jiskoot, H., et al. (2005). Multispectral imaging contributions to global land ice measurements from space. *Remote Sensing of Environment*, *99*, 187–219. http://dx.doi.org/10.1016/j.rse.2005.07.004.

Marmion, M., Hjort, J., Thuiller, W., & Luoto, M. (2008). A comparison of predictive methods in modelling the distribution of periglacial landforms in Finnish Lapland. *Earth Surface Processes and Landforms*, *33*, 2241–2254. http://dx.doi.org/10.1002/esp.1695.

Moguerza, J. M., & Muñoz, A. (2006). Support vector machines with applications. *Statistical Science*, *21*(3), 322–336. http://dx.doi.org/10.1214/088342306000000493.

Mountrakis, G., Im, J., & Ogole, C. (2011). Support vector machines in remote sensing: A review. *ISPRS Journal of Photogrammetry and Remote Sensing*, *66*, 247–259. http://dx.doi.org/10.1016/j.isprsjprs.2010.11.001.

Paul, F., Huggel, C., & Kääb, A. (2004). Combining satellite multispectral image data and a digital elevation model for mapping of debris-covered glaciers. *Remote Sensing of Environment*, *89*(4), 510–518. http://dx.doi.org/10.1016/j.rse.2003.11.007.

Peters, A., & Hothorn, T. (2009). ipred: Improved predictors. R package version 0.8-8. http://CRAN.R-project.org/package=ipred

Piatek, J. L. (2009). Thermophysical properties of terrestrial rock and debris-covered glaciers as analogs for Martian lobate debris aprons. *40th Lunar and Planetary Science Conference, (Lunar and Planetary Science XL), held March 23–27, 2009 in The Woodlands, Texas* id. 2127.

Quinn, P., Beven, K., Chevallier, P., & Planchon, O. (1991). The prediction of hillslope flow paths for distributed hydrological modelling using digital terrain models. *Hydrological Processes*, *5*, 59–79.

R Development Core Team (2010). *R: A language and environment for statistical computing.* Vienna, Austria: R Foundation for Statistical Computing3-900051-07-0. http://www.R-project.org/

Recio-Recio, J. A., Ruiz-Fernández, L. A., & Fernández-Sarriá, A. (2005). Use of Gabor Filters for texture classification of digital images. *Física de la Tierra*, *17*, 47–56.

Ruß, G., & Brenning, A. (2010a). Data mining in precision agriculture: Management of spatial information. *Lecture Notes in Computer Science*, *6178*, 350–359. http://dx.doi.org/10.1007/978-3-642-14049-5_36.

Ruß, G., & Brenning, A. (2010b). Spatial variable importance assessment for yield prediction in precision agriculture. *Lecture Notes in Computer Science*, *6065*, 184–195. http://dx.doi.org/10.1007/978-3-642-13062-5_18.

Shukla, A., Arora, M. K., & Gupta, R. P. (2010). Synergistic approach for mapping debris-covered glaciers using optical–thermal remote sensing data with inputs from geomorphometric parameters. *Remote Sensing of Environment*, *114*(7), 1378–1387. http://dx.doi.org/10.1016/j.rse.2010.01.015.

Sing, T., Sander, O., Beerenwinkel, N., & Lengauer, T. (2009). ROCR: Visualizing the performance of scoring classifiers. R package version 1.0-4. http://CRAN.R-project.org/package=ROCR

Strobl, C., Boulesteix, A. -L., Zeileis, A., & Hothorn, T. (2007). Bias in random forest variable importance measures: Illustrations, sources and a solution. *BMC Bioinformatics*, *8*, 25. http://dx.doi.org/10.1186/1471-2105-8-25.

Xiao, P., Feng, X., An, R., & Zhao, S. (2010). Segmentation of multispectral high-resolution satellite imagery using log Gabor filters. *International Journal of Remote Sensing*, *31*(6), 1427–1439. http://dx.doi.org/10.1080/01431160903475324.

Zevenbergen, L. W., & Thorne, C. R. (1987). Quantitative analysis of land surface topography. *Earth Surface Processes and Landforms*, *12*, 47–56.

Zweig, M. H., & Campbell, G. (1993). Receiver-operating characteristic (ROC) plots. *Clinical Chemistry*, *39*, 561–577.